Article

Cell-Selective Cytotoxicity of a Fluorescent Rhodium Metalloinsertor Conjugate Results from Irreversible DNA Damage at Base Pair Mismatches

Adela Nano, Julie M. Bailis, Natalie F. Mariano, Elizabeth D. Pham, Stephanie D. Threatt, and Jacqueline K. Barton

Biochemistry, **Just Accepted Manuscript** • Publication Date (Web): 22 Jan 2020

Cell-Selective Cytotoxicity of a Fluorescent Rhodium Metalloinsertor Conjugate Results from Irreversible DNA Damage at Base Pair Mismatches

Adela Nano,[†#] Julie M. Bailis,[‡#] Natalie F. Mariano,[‡] Elizabeth D. Pham,[‡] Stephanie D. Threatt,[†] and Jacqueline K. Barton[†*]*

[†] Division of Chemistry and Chemical Engineering, California Institute of Technology, Pasadena, CA 91125

[‡] Department of Oncology Research, Amgen Research, Amgen, Inc., South San Francisco, CA 94080

[#] These authors contributed equally to the work.

* To whom correspondence should be addressed. Julie M. Bailis, Email: jbailis@amgen.com; Telephone: +1 (650) 244 2361, and Jacqueline K. Barton, Email: jkbarton@caltech.edu; Telephone: +1 (626) 395-6075.

ABSTRACT: Up to twenty percent of solid tumors are characterized by DNA mismatch repair (MMR) deficiency and microsatellite instability (MSI) that confer resistance to standard of care chemotherapy. MMR-deficient cancers have an increased mutation rate and accumulate DNA mismatches. We previously described a class of compounds, rhodium metalloinsertors, that bind DNA mismatches with high specificity and selectivity and have potential as targeted therapy. $[Rh(chrysi)(phen)(PPO)]^{2+}$ (RhPPO) is the most potent, selective compound in this class and acts by targeting DNA mismatches, resulting in preferential cytotoxicity to MMR-deficient cancers. To explore further the cellular mechanism of action of RhPPO, we conjugated the metal complex to a fluorescent probe, cyanine 3 (Cy3). RhPPO-Cy3 binds DNA mismatches and retains the selectivity and potent cytotoxic activity of RhPPO for MMR-deficient cell lines. RhPPO-Cy3 forms discrete foci in the cell nucleus that overlap with sites of DNA damage, suggesting that the lesions occur at or near DNA mismatch sites. RhPPO-Cy3 foci persist over time, despite initial processing of the lesion and recruitment of repair proteins, consistent with the idea that the complex binding to a mismatch prevents repair. RhPPO-Cy3 binding does not lead to activation of p53 and the apoptotic pathway. Together, these findings support the idea that RhPPO-Cy3 binding leads to irreversible DNA damage at DNA mismatches that enables selective cytotoxicity to MMR-deficient cells.

INTRODUCTION

DNA mismatch repair (MMR) is a key mechanism that detects and repairs mismatched DNA base pairs that arise during DNA replication or from exposure to DNA damaging agents.[1,2,3] Cells with impaired MMR ability accumulate mutations and develop genome instability that can cause or contribute to cancer. MMR is a complex molecular system where the MLH1/PMS2 and MSH2/MSH6 heterodimers recognize and bind DNA mismatches and recruit repair enzymes to excise and replace mismatched bases. Inactivation of any of the MMR genes by somatic or germline mutation or by epigenetic silencing results in a deficient MMR pathway.[3,4,5] Deficiencies in the MMR machinery are associated with an increased mutation rate (100- to 1000-fold) and occur in 15% of colorectal cancer (CRC) and up to 20% of many solid tumors.[6-10] It is well established that CRC patients with MMR-deficient tumors do not respond to standard care chemotherapy such as 5-fluorouracil, cisplatin, temozolomide, or pyrimidine analogues.[11,12] In the last few years, MMR-deficient CRC, as well as other MMR-deficient cancers, have shown remarkable response to immunotherapy with anti-programmed death-1 (PD-1) antibodies.[13,14] However, many patients relapse over time,

and durability of response is likely to require combination therapy.[15, 16] Therefore, new therapies are still needed for effective treatment of MMR-deficient cancers.

The high mutation rate of MMR-deficient cancers leads to heterogeneity that is challenging to target therapeutically. We have proposed targeting the state of MMR deficiency, and specifically DNA mismatches, as a strategy for selective killing of MMR-deficient cancer cells.[17,18] Rhodium metalloinsertors are a class of compounds that bind DNA mismatches with high specificity and selectivity[18, 19, 20] Thermodynamic destabilization at a mismatch site allows the compounds to insert *via* the aromatic chrysi (5,6-chrysenequinone diimmine) ligand into the DNA through the minor groove. This binding mode is non-covalent but ejects the mismatched base pairs outside of the DNA helix, generating DNA lesions that activates the DNA damage response and drives selective killing of MMR-deficient cells.[18,20]

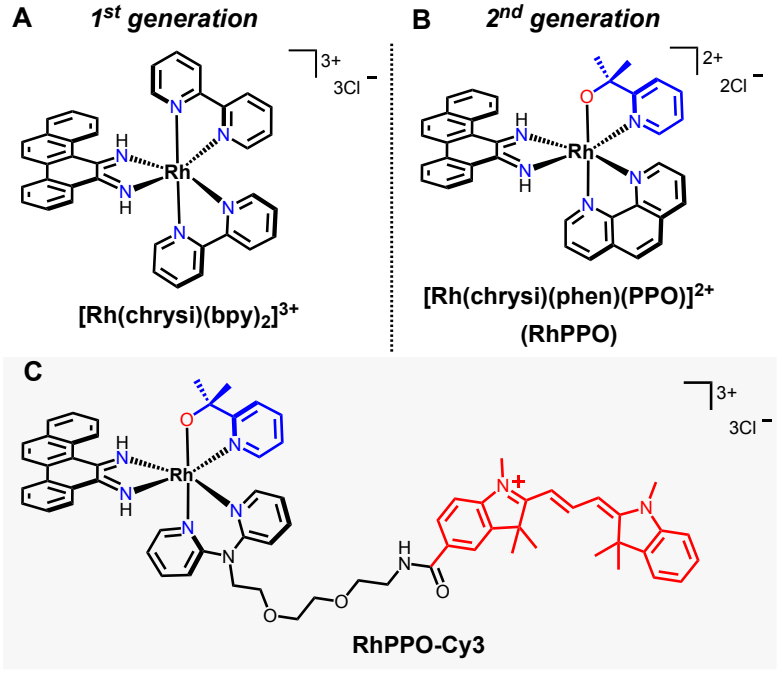

Chart 1. Chemical structures of compounds used in this study. **(**A**)** RhPPO, a second generation metalloinsertor, (B) $[Rh(chrysi)(bpy)_2]Cl_3$, representing the first generation of metalloinsertors, (C) RhPPO-Cy3 conjugate which, in the presence of mismatched DNA, emits light through its cyanine3 fluorophore; the PPO ligand is shown in blue, and Cy3 fluorophore is shown in red.

We have described a second generation of rhodium metalloinsertors where one of the bidentate ligands is metalated *via* a rhodium-oxygen bond, which differs from the first generation of rhodium metalloinsertors that employ N^N coordination (Chart 1).[21,22] This new ligand coordination reduces the total charge of the metal complex from +3 to +2 and has a direct consequence on the pKa of immine protons on the chrysi ligand and therefore bulk of the chrysi ligand. The lead compound in this series, $[Rh(phen)(chrysi)(PPO)]^{2+}$ (RhPPO) demonstrates remarkably high cellular potency and selectivity towards MMR-deficient cells relative to the first generation of compounds.[22,23] These findings were extended to a panel of 27 CRC cell lines, where RhPPO demonstrated preferential cytotoxic activity in the MMR-deficient cell lines relative to the MMR-proficient cell lines.[24] Specifically, RhPPO cytotoxic activity showed a strong correlation with the level of DNA mismatches present in the cells, as detected with a fluorescent rhodium conjugate, RhCy3.[24,25] These findings strongly suggested that the cellular target of RhPPO is a DNA mismatch.

The mechanism that drives the high cellular potency of RhPPO is not well understood. RhPPO causes DNA lesions that lead to cell death primarily by necrosis, which is distinct from the mechanism of cisplatin and other DNA-damaging drugs that induce cell death primarily through apoptosis.[26,27] Our first-generation rhodium conjugate, RhCy3, emits a fluorescent signal in cells with DNA mismatches and functions primarily as a diagnostic probe.[25] In the present study, we characterize a fluorescent conjugate of RhPPO, RhPPO-Cy3, which not only acts as a probe that binds DNA mismatches but also functions to promote cytotoxicity of MMR-deficient cells. RhPPO-Cy3 binding to DNA mismatches is visualized as discrete foci in the nucleus of live cells, enabling mechanism of action studies that further explore the nature of the DNA lesions caused by PPO-based metalloinsertor compounds. We find that RhPPO-Cy3 binding causes DNA breaks and activates the DNA damage response. The RhPPO-Cy3 foci overlap with DNA damage foci that contain phosphorylated histone H2AX (phospho-H2AX) and Rad51, suggesting that the DNA breaks occur at the DNA mismatch site and undergo initial resection. However, although cell cycle progression appears blocked after RhPPO-Cy3 binding, cells do not activate the p53/p21 axis that would trigger cyclin-dependent kinase (CDK)-dependent cell cycle arrest and initiation of apoptosis. Instead, the Rh-PPO foci persist, indicating rhodium-bound DNA mismatches are not repaired, and the cells undergo cell death by necrosis. Together these findings suggest that the DNA lesions induced by RhPPO-Cy3 binding occur at

the mismatched base pair and that the cellular context of this DNA damage prevents its recognition by the DNA repair or apoptotic machinery.

MATERIALS AND METHODS

Materials. All reactions except when mentioned were performed under a dry atmosphere of argon. $[Rh(NH_3)_5Cl]Cl_2$ was purchased from Strem Chemical, Inc. (Newburyport, MA), 2,2′-dipyridylamine (HDPA), 1,2-bis(2-iodoethoxy)ethane, anhydrous $^{i}Pr_2NH$, anhydrous DMF, (2-(1H-benzotriazol-1-yl)-1,1,3,3-tetramethyluronium hexafluorophosphate (HBTU) and Sephadex ion exchange resin were obtained from Sigma-Aldrich and used as purchased. Sep-Pak C18 solid phase extraction cartridges were purchased from Waters Chemical Co. (Milford, MA). Flash chromatographic purifications were performed using 40-63 μm silica gel or Sep-Pak C18 cartridges. HPLC purifications were performed on an HP1100 high-pressure liquid chromatography system equipped with a diode array detector using a Varian DynaMax C18 semi-preparative column. Mass spectrometry was performed at the California Institute of Technology mass spectrometry facility. UV-vis absorption spectra were recorded on a Cary 100 Bio spectrophotometer. ^{1}H, ^{13}C NMR spectra were recorded on a Bruker Spectrometers (400 or 300 MHz). ^{1}H, ^{13}C chemical shifts were reported to the delta scale in ppm relative to the residual peak of the deuterated used solvent as internal standards: chloroform-d_1 (^{1}H: δ = 7.26 ppm; ^{13}C: δ = 77.16 ppm), methanol-d_4

(^{1}H: δ = 3.31 ppm; ^{13}C: δ = 49.00 ppm), acetonitrile-d_3 (^{1}H: δ = 1.94 ppm; ^{13}C: δ = 118.26 ppm).

Synthesis and characterization of RhPPO-Cy3 conjugate. The 2-(pyridine-2-yl)propan-2-ol **(PPO)** ligand and **DPA-Cy3** were prepared according to previously reported procedures.[21,25] $[Rh(chrysi)(NH_3)_4]Cl_3$ was obtained from reacting $[Rh(NH_3)_6](OTf)_3$ and 5,6-chrysenquinone according to published procedures.[28]

Synthesis of RhDPA-Cy3. A Schlenk flask was charged with $[Rh(chrysi)(NH_3)_4]Cl_3$ (0.091 mmol, 80 mg) and DPA-Cy3 (0.111 mmol, 90 mg) and the solids were dissolved with a water/acetonitrile/ethanol (2/3/3 ml) mixture. The solution was degassed with argon for about 30 - 40 minutes and the Schlenk flask was refluxed at 95°C for 20 hours. Afterwards, the solution was cooled to ambient temperature and loaded on a QAE Sephadex anion exchange column equilibrated with 0.1 M $MgCl_2$ aqueous solution. The collected solution was concentrated under vacuum and purified using a Waters Sep-Pak C_{18} SiO_2 column. The column was first eluted with H_2O/ACN (10%) allowing the elimination of unreacted starting materials while the desired product sticks to the top which is then eluted with H_2O (0.1 % TFA)/ ACN 25%. The collected pure fractions were lyophilized yielding the product as dark red solids (68 mg, 61%). **NMR ^{1}H** (400 MHz, Acetonitrile-d_3) δ 9.12 (d, J = 5.1 Hz, 1H), 9.05 (d, J = 5.8 Hz, 1H), 8.80 (d, J = 8.5 Hz, 1H), 8.57 (d, J = 6.5 Hz, 1H), 8.26 (t, J = 13.5 Hz, 1H), 8.10 – 7.98 (m, 2H), 7.92 (d, J = 8.8 Hz, 1H), 7.85 – 7.79 (m, 2H), 7.77 (d, J = 8.9 Hz, 1H), 7.70 – 7.64

(m, 1H), 7.57 – 7.41 (m, 7H), 7.38 (dd, *J* = 7.8, 1.2 Hz, 1H), 7.36 – 7.31 (m, 1H), 7.29 (dd, *J* = 7.4, 1.4 Hz, 1H), 7.22 – 7.13 (m, 2H), 7.09 (d, *J* = 1.7 Hz, 1H), 6.83 – 6.76 (m, 2H), 6.51 (d, *J* = 8.3 Hz, 1H), 6.21 (d, *J* = 13.7 Hz, 1H), 6.11 (d, *J* = 13.3 Hz, 1H), 4.20 (p, *J* = 3.8 Hz, 2H), 4.08 (s, 4H), 3.77 (s, 3H), 3.55 (d, *J* = 25.5 Hz, 2H), 3.45 (s, 3H), 3.33 (s, 3H), 3.24 (d, *J* = 6.4 Hz, 1H), 3.10 (s, 2H), 2.97 (dt, *J* = 9.8, 4.9 Hz, 2H), 1.55 (s, 6H), 1.45 (s, 3H), 1.41 (s, 3H). **^{13}C NMR** (101 MHz, Acetonitrile-d_3) δ 176.8, 175.3, 174.6, 167.5, 160.7, 160.4, 155.2, 155.0, 153.8, 153.5, 151.2, 145.7, 143.4, 143.2, 143.1, 141.7, 140.7, 137.2, 136.3, 136.2, 134.5, 134.2, 131.2, 131.1, 130.7, 130.5, 129.9, 129.4, 129.4, 129.0, 128.5, 126.5, 126.2, 126.2, 123.2, 122.9, 122.9, 122.5, 121.5, 120.8, 119.0, 118.4, 115.7, 112.2, 110.6, 104.2, 102.9, 71.0, 70.4, 70.2, 67.0, 51.9, 50.2, 49.2, 39.8, 32.1, 27.7, 27.4. **TOF-MS ESI** calculated *m*/*z* = 1225.3816 for $[M - 2H + OTf]^+$, found 1225.3796; calculated *m*/*z* = 538.2148 for $[M - H]^{2+}$, found 538.2071.

Synthesis of RhPPO-Cy3. A Schlenk flask was charged with water (2 mL) and degassed with argon for about 40 minutes. **RhDPA-Cy3** (34 mg, 0.027 mmol) was loaded into the solution and 2 mL of ethanol were additionally added. After degassing the solution for 5 more minutes, **PPO** ligand (6.0 mg, 0.044 mmol) was finally added and the reaction mixture was allowed to stir at 95°C overnight. After cooling to ambient temperature, the crude was concentrated under vacuum and loaded on a Sep-Pak C_{18} SiO_2 column for purification. Additional purifications were performed using HPLC, thus yielding the product as dark-red solids (6 mg, 17%). **NMR ^{1}H** (400 MHz, Acetonitrile-d_3) δ 8.53 – 8.42 (m, 2H), 8.31 – 8.29 (m, 3H), 8.15 – 8.07 (m, 1H), 7.95 (d, *J* =

1.7 Hz, 1H), 7.88 (dd, *J* = 8.3, 1.7 Hz, 1H), 7.65 (ddd, *J* = 8.5, 7.2, 2.0 Hz, 2H), 7.60 – 7.54 (m, 3H), 7.54 – 7.44 (m, 3H), 7.43 – 7.33 (m, 5H), 7.33 – 7.28 (m, 1H), 7.25 (d, *J* = 8.3 Hz, 1H), 7.19 (d, *J* = 8.4 Hz, 1H), 6.97 (ddd, *J* = 7.3, 5.0, 0.9 Hz, 2H), 6.43 (d, *J* = 13.8 Hz, 1H), 6.38 (d, *J* = 13.6 Hz, 2H), 6.30 (dd, *J* = 13.3, 3.5 Hz, 2H), 4.31 (t, *J* = 6.2 Hz, 2H), 3.74 (t, *J* = 6.2 Hz, 2H), 3.66 (s, 2H), 3.65 – 3.61 (m, 6H), 3.59 (d, *J* = 2.8 Hz, 2H), 3.56 – 3.49 (m, 4H), 1.76 (s, 3H), 1.75 (s, 3H), 1.74 (s, 6H), 1.74 (s, 6H). **TOF-MS ESI** calculated *m*/*z* = 1177.4449 for $[M - 2H]^+$, found 1177.3186; calculated *m*/*z* = 589.7300 for $[M - H]^{2+}$, found 589.7303. **UV-vis** (in Tris 5 mM, 200 mM NaCl, pH 7.4): λ(552nm) ε = 61,000 M^{-1} cm^{-1}; λ(267nm) ε = 28,000 $M^{-1}cm^{-1}$.

Photophysical measurements. Luminescence spectra were recorded using a QE Pro High Performance Spectrometer with a back-thinned, TE-cooled CCD detector controlled by the OceanView data acquisition and analysis software package (Ocean Optics, Inc.). Sample excitation was provided by a 455 nm LED (Thorlabs model M455L2). The emission spectra were recorded in Tris buffer solution (5 mM Tris, 200 mM NaCl, pH 7.4) at 25°C using a water circulation system. Excitation wavelength was λ_{Ex} = 455 nm and the emission integral was reported after each addition of DNA, as a scalar function from 548 to 675 nm. The flourescence titrations were performed twice for the mismatched (MM) DNA and once for the well-matched (WM) DNA. The dsDNA was a 27-mer sequence, 5′-GAC CAG CTT ATC A***C***C CCT AGA TAA GCG-3′ where the complementary MM strand comprises a (***C***) at the mismatched site *versus* (***G)*** for WM.

The RhPPO-Cy3 fluorescence titrations with increasing amounts of MM dsDNA were used to determine the binding affinity of the conjugate with the mismatched DNA duplex. [DNA] was considered as concentration of mismatches on the full-length fragments, *i.e.* the 27-mer oligonucleotide. The plotted data were fit to a one-site specific binding equation curve with GraphPad Prism 7.

Cell culture. HCT-116 N and HCT-116 O cells[29] were grown in Roswell Park Memorial Institute (RPMI) 1640 medium supplemented with 10% fetal bovine serum (FBS), 2 mM L-glutamine, 0.1 mM nonessential amino acids, 1 mM sodium pyruvate, 100 μg/mL penicillin, 100 μg/mL streptomycin, and 400 μg/mL geneticin (G418). MMR-deficient cell lines Lovo, DLD-1, SW48, RKO and KM12, and MMR-proficient cell lines LS1034, Colo320, SW948, SW1463 and SW837 were obtained from the American Type Culture Collection (ATCC) and grown in RPMI media with 10% FBS and 1% penicillin/streptomycin. Cells were maintained in tissue culture flasks (Corning Costar) at 37°C under 5% CO_2 in a humidified atmosphere.

Cell viability. Cells were plated in 96-well plates at 5000 cells/well in a volume of 90 μl. Cells were incubated for 6 hours at 37°C, 5% CO_2 prior to adding compound. The cells were then treated with RhPPO-Cy3 or cisplatin in a dose range, using a 1:2 dilution series of 12 points, and incubated for 48 hours at 37°C. The assay plate was equilibrated to room temperature for 15 minutes, and then cytotoxicity was assayed using a CellTiter-Glo assay (Promega), performed according to the manufacturer's

instructions. The luciferase signal was recorded on a Biotek Neo2 plate reader or a FlexStation 3 Multi-Mode plate reader. Percent viability was determined by the ratio of the luminescence of treated cells compared to untreated cells. EC_{50} values were determined by fitting the cell viability data points to a dose-response curve in GraphPad Prism 7. Experiments were performed in duplicate in at least three independent experiments.

Live cell images and colocalization studies. HCT-116 O cells were plated at 7000 cells/well in 96-well plates (Greiner). Cells were incubated for 5 hours prior to adding compound at the concentrations indicated. The cells with compound were then incubated for 48 hours before analysis. For live cell imaging, 1 μM Hoechst dye (Thermo Fisher) was added to cells and incubated at 37°C for 90 minutes. Cells were imaged on an Opera Phenix (Perkin Elmer) using 63x magnification. Cells were also fixed and permeabilized to enable colocalization studies. Cells were fixed in 4% paraformaldehyde and 0.5% Triton-X for 15 minutes. Then, the supernatant was aspirated off. Cells were blocked with biotin, according to manufacturer's protocol (Thermo Fisher), and then incubated with 1X blocking buffer (Thermo Fisher) for an additional 30 minutes. Cells were incubated with primary antibodies for 60 minutes at ambient temperature, protected from light. Primary antibodies used were: anti-phospho-H2AX (Millipore), anti-Rad51 (Cell Signaling), and anti-Cy3-biotin (Sigma). The anti-Cy3-biotin antibody was used to amplify the Cy3 signal on the RhPPO-Cy3

molecule, which otherwise underwent photobleaching during additional antibody staining. After incubation with primary antibodies, cells were washed three times with phosphate-buffered saline (PBS). Secondary antibodies against phospho-H2AX (1:100, Millipore) and Streptavidin AF647 (1:1000, Thermo Fisher) were incubated with cells for 45 minutes at room temperature. Hoechst dye (1 μg/ml; Sigma) was used to visualize the cell nuclei. Cells were then washed three times in PBS and then maintained in PBS with the plates sealed. Cells were imaged using an Opera Phenix (Perkin Elmer) using 63x magnification.

Image analysis was carried out using Acapella (Perkin Elmer) following image acquisition. Hoechst staining was used to define the cell nucleus, and then RhPPO-Cy3 foci within the nucleus were identified based on intensity of the AF647 signal. Overlap of this signal with the AF488 channel was used to evaluate colocalization with pH2AX or Rad51

Comet assay. DNA damage was evaluated using a neutral Comet assay (Cell Biolabs), performed according to the manufacturer's instructions. Cells were treated with compound as indicated, and then collected using a cell scraper, mixed with melted agarose, and pipetted onto slides. The samples were denatured and then analyzed by Tris-borate-EDTA (TBE) gel electrophoresis at 35 V for 60 minutes to separate DNA fragments from intact DNA. The samples were then stained with Vista Green

fluorescent dye to visualize the cellular DNA and imaged using an EVOS cell imaging system (Thermo Fisher).

Western blots. HCT-116 N and HCT-116 O cells were treated with compound as indicated for 24 hours at 37°C. Cell pellets were then collected by non-enzymatic cell dissociation buffer (Thermo Fisher) and protein lysates were prepared in RIPA buffer (Pierce) containing a protease and phosphatase inhibitor cocktail (Thermo Fisher). Total lysate (40 μg) in running dye (Thermo Fisher) was incubated at 95°C for 5 minutes. Samples were then loaded onto a 4-12% NuPAGE SDS Gel (Thermo Fisher) and analyzed by electrophoresis for 60 minutes at 120 V.

The iBlot2 Dry Blotting System (Thermo Fisher) was used to transfer proteins from the NuPAGE SDS Gel to a nitrocellulose membrane. Proteins were transferred using the following protocol: 1 minute at 20 V, 4 minutes at 23 V, 2 minutes at 25 V. After transfer, the membrane was pre-wet in 1X Tris-buffered saline (TBS) for 2 minutes and then blocked with TBS Blocking Buffer (Odyssey) for 1 hour at ambient temperature with gentle shaking. The membrane was incubated with primary antibodies, phospho-p53 (serine 15) and p21 Waf1/Cip1 (Cell Signaling Technology) at 1:1000 in blocking buffer + 0.2% Tween 20, overnight at 4°C with gentle shaking. The membrane was then washed 3X with 1X-TBS + 0.1%Tween 20 (TBS-T) at ambient temperature for 5 minutes. The membrane was incubated with appropriate secondary antibody coupled to IRDye-700 or IRDye-800 (LiCOR) at 1:10,000 in blocking buffer +

0.2% Tween 20, at ambient temperature for 1 hour with gentle shaking. The membrane was then washed 3 times with 1X TBS-T and imaged with an Odyssey CLx (LiCOR).

RESULTS

Synthesis and characterization of a RhPPO-Cy3 conjugate. To further investigate the cellular mechanism of action of RhPPO, we synthesized a fluorescent analogue, the cyanine conjugate RhPPO-Cy3. RhPPO-Cy3 was designed to enable visualization of the molecule binding to DNA and interactions on chromatin, with similar potency and cell selectivity as the unconjugated molecule, RhPPO. As illustrated in Scheme 1, the fluorophore is appended on the dipyridyl ligand through a polyethylene glycol (PEG) linker, leaving the PPO ligand intact. The synthesis procedure for DPA-Cy3 was previously described and reported in literature.[25] RhPPO-Cy3 was prepared following the synthesis approach indicated in Scheme 1, inspired by the previously reported RhCy3 conjugate.[25] Briefly, DPA-Cy3 was refluxed with $[Rh(Chrysi)NH_3)_4]^{3+}$ under anaerobic conditions giving RhDPA-Cy3 in good yields. Finally, PPO substitution of the ammonia ligands via an N^O coordination yielded the corresponding RhPPO-Cy3 complex. Since ammonia is a strong ligand, the rhodium ammine complexes are relatively stable, therefore explaining in part the low yield of the final reaction. Additionally, side reactions occur given the reactivity of rhodium complexes and the reaction conditions. During our preliminary results we noticed that

complexation of PPO with $[Rh(chrysi)(NH_3)_4]^{3+}$ yielded preferentially the bis-coordinated species instead of the mono-coordinated rhodium-PPO complex (data not shown). Given these observations and others not reported here, we proceeded first with DPA-Cy3 complexation, followed by PPO ligand coordination.

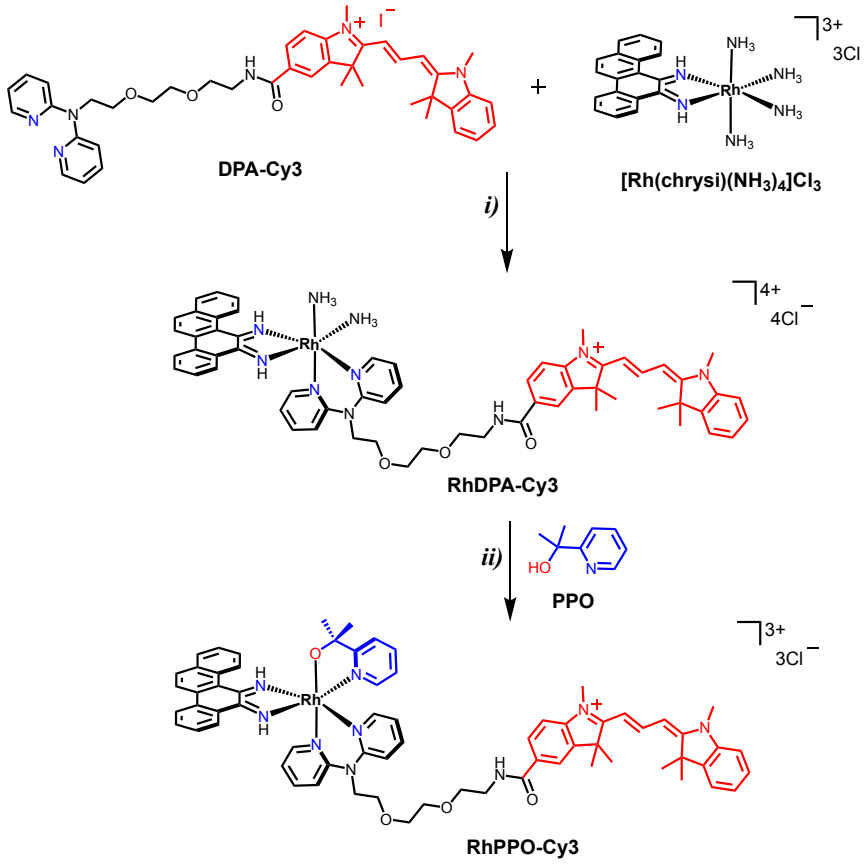

Scheme 1. Synthesis pathway for RhPPO-Cy3 conjugate. *i*) *ii*) EtOH/ACN/H_2O, 95°C, overnight under anaerobic conditions followed by anion exchange using 0.1 M $MgCl_2$. The synthesis of DPA-Cy3 and $[Rh(chrysi)(NH_3)_4]$ has been previously reported.[25, 28]

After HPLC purification, the compound was characterized using standard NMR techniques and high-resolution mass spectrometry; all the spectra are included in the Supplemental Information (Figures S1-S7). The RhPPO-Cy3 conjugate is soluble in aqueous solution. Its absorption spectrum corresponds to the sum of the absorption of the parent metal complex and Cy3 (Supplemental Information, Figure S8). Additionally, the presence of a large band at 430 nm marks charge transfer from the rhodium center to the chrysi ligand and reflects the protonated state of immines on the chrysi ligand.[22] After photoexcitation at 455 nm, RhPPO-Cy3 yields a weak luminescence centered at 567 nm. The luminescence is increased and the maximum emission is slightly red shifted by 5 nm when RhPPO-Cy3 is incubated with a 27-mer double-stranded DNA (dsDNA) containing a single CC mismatch (Figure S8, Supplemental Information). This enhancement confirms that RhPPO-Cy3 binds mismatched dsDNA.

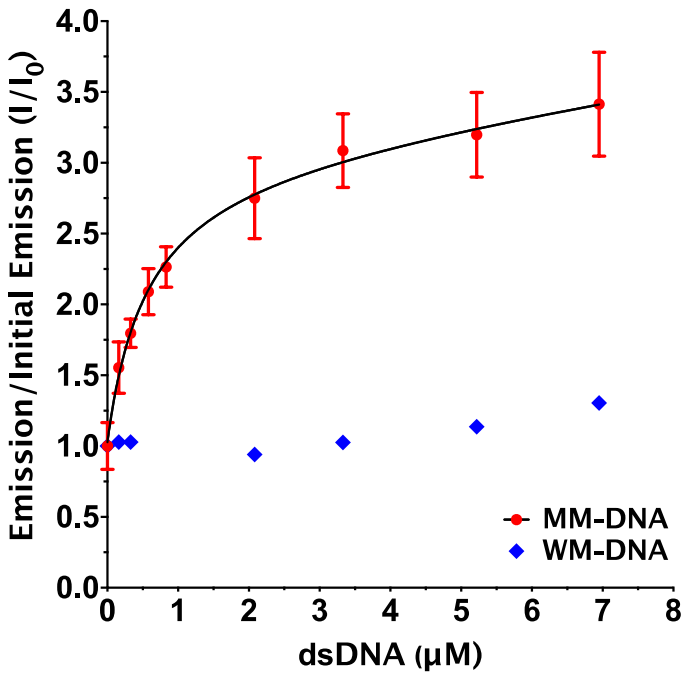

Figure 1. Fluorescence titrations with increasing amounts of WM DNA (blue) or MM DNA (red). [RhPPO-Cy3] = 2 μM, in Tris buffer (5mM Tris, 200 mM NaCl, pH = 7.4) at 25°C. λ_{Ex} = 455 nm, emission recorded from 548-675 nm. I_0 is the integrated emission of RhPPO-Cy3 solution without DNA and, I represents the emission integral from 548-675 nm as a scalar function measured after each addition of DNA. The 27-mer DNA sequence: 5'-GAC CAG CTT ATC A**C**C CCT AGA TAA GCG-3' where the MM strand comprises a (***C***) at the mismatched site *vs.* (**G**) for WM. The titration points were fit to a one site – total binding equation using GraphPad Prism 7. Error bars represent the ratio of the standard deviation to the mean of duplicates.

RhPPO-Cy3 binds mismatched DNA with high affinity and specificity. For mechanistic studies, it was important that RhPPO-Cy3 have similar binding affinity to

that of the parent RhPPO molecule, although the RhPPO-Cy3 conjugate contains a PEG linker and an indocyanine fluorophore. Therefore, we examined the DNA binding affinity, K_B, of RhPPO-Cy3 to duplex DNA with and without a single base mismatch through fluorescence titrations. The binding affinity defines the interaction strength between the duplex DNA and the fluorescent probe and is experimentally measured through the dissociation constant $K_d = 1/ K_B$.[29] Thus, a 2 μM Tris buffer solution of the fluorescent probe was titrated with increasing amounts of 27-mer dsDNA containing a central CC base-paired mismatch. While an increase in emission intensity is seen in the presence of mismatched (MM) dsDNA, negligible fluorescence intensity was observed with well matched (WM) dsDNA (Figure 1). This change in fluorescence intensity can be used to determine the dissociation constant by plotting the ratio of the fluorescence intensity versus the concentration of the duplex DNA. The data are then analyzed via a nonlinear fitting, using a one site binding – total equation, yielding a K_d of 0.55 ± 0.1 μM for the duplex containing a CC mismatch. Given the K_d value, the resulting binding affinity of RhPPO-Cy3 to the mismatched DNA sequence is $K_B(CC) = 1.8 \times 10^6\ M^{-1}$, which is comparable to that of other Rh–O metalloinsertors lacking the fluorescent tag, where the $K_B(CC)$ ranges from $1.5 – 9.2 \times 10^6\ M^{-1}$.[21,22] In the current proof-of-concept study, we used only a duplex DNA containing a CC mismatch to evaluate the binding affinity of RhPPO-Cy3 versus that of the parent RhPPO complex. However, binding affinities of Rh–O metalloinsertors at all possible DNA mismatches have been

determined and reported to correlate directly with thermodynamic destabilization of the mismatch site.[22] Additionally, fluorescence titrations were performed also in the presence of increasing amounts of well-matched dsDNA, but little variation in fluorescence intensity was observed. Overall, these results indicate that appending the cyanine fluorophore through a small PEG linker on the dipyridyl ligand does not have a significant impact on the specific DNA binding affinity of RhPPO-Cy3.

RhPPO-Cy3 is cytotoxic to MMR-deficient cells. The activity of RhPPO-Cy3 was evaluated in isogenic HCT-116 cell lines HCT-116 O, which is MMR-deficient due to homozygous mutation lacking MLH1, and HCT-116 N which is MMR-proficient due to the presence of an additional copy of Chromosome III that expresses wild type MLH1.[30,31] RhPPO-Cy3 preferentially decreased cell viability of HCT-116 O cells, with a half-maximal effective concentration (EC_{50}) of 1.0 ± 0.1 μM (Figure 2). In contrast, the same concentration showed less cell killing (≤10%) against the MMR-proficient HCT-116 N cells, where the EC_{50} was 1.9 ± 0.2 μM. RhPPO-Cy3 activity increased over time, with maximal activity by 72 hours (Figure 3; Supplemental Information, Figure S9). The preferential cytotoxicity of RhPPO-Cy3 for MMR-deficient cells was also observed against other CRC cell lines (Supplemental Information, Figure S10).[24] Overall, RhPPO-Cy3, like the unconjugated parental compound RhPPO, shows potency and selectivity for MMR-deficient cells, indicating that it is a suitable candidate for studies of compound localization and cellular mechanism of action.

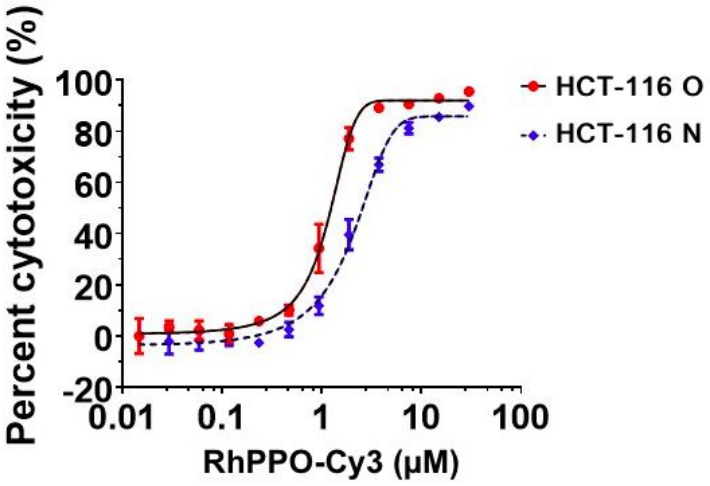

Figure 2. RhPPO-Cy3 is preferentially cytotoxic to MMR-deficient HCT-116 O cells. HCT-116 O and HCT-116 N cells were treated with RhPPO-Cy3 in a 12-point dose response. After 72 hours incubation, cell viability was assessed with a Cell Titer-glo assay. The graph shows data for duplicate samples from a representative assay.

RhPPO-Cy3 forms foci in the cell nucleus that overlap with DNA damage foci. The cellular localization of RhPPO-Cy3 was evaluated by live cell imaging in HCT-116 O and HCT-116 N cells. Cells were treated with 5 μM RhPPO-Cy3, a concentration higher than the cell EC_{90}, for 24 hours and then visualized for Cy3 fluorescence. Cellular uptake of the compound was observed, with RhPPO-Cy3 foci evident both in the cell nucleus and around the periphery of the nuclear membrane (Figure 3A). Nuclear RhPPO-Cy3 foci were observed in the MMR-deficient HCT-116 O cells, consistent with the idea that the complex binds to genomic DNA mismatches.

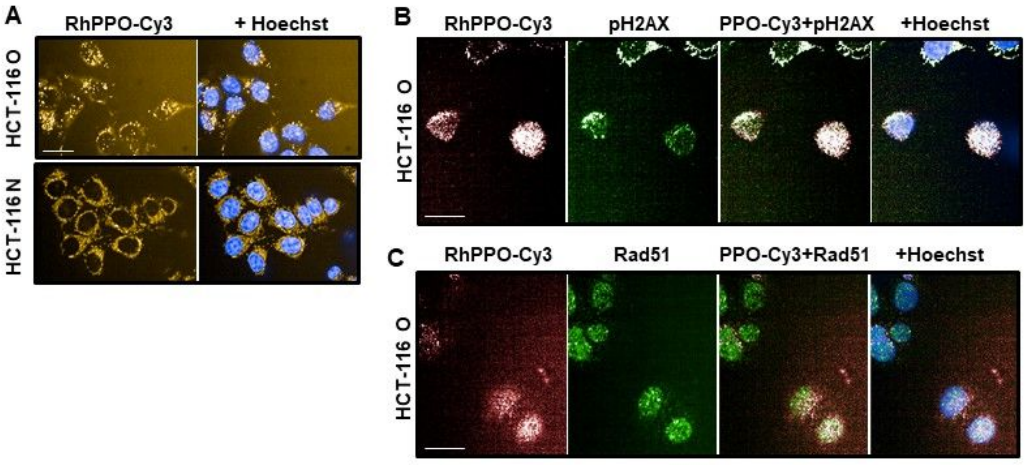

Figure 3. RhPPO-Cy3 forms nuclear foci that overlap with DNA damage foci. HCT-116 O and HCT-116 N cells were treated with RhPPO-Cy3, and RhPPO-Cy3 localization was evaluated in live cells (A), or with DNA damage markers phospho-H2AX (B) or Rad51 (C) in fixed, permeabilized cells. Cells were counterstained with Hoechst dye to detect the cell nuclei. Scale bar, 20 μm. In Figure 3B and 3C (third image) RhPPO-Cy3 is abbreviated as PPO-Cy3.

The selective cytotoxicity of the parent compound, RhPPO, is associated with the formation of nuclear foci that contain phospho-H2AX, a marker for DNA double-strand breaks (DSBs).[23] The fluorescence of RhPPO-Cy3 conjugate enabled us to assess whether the DNA damage foci marked by phospho-H2AX occurred at sites of rhodium metalloinsertor binding. We initially treated cells with 5 μM RhPPO-Cy3 for 24 hours, imaged the fluorescent cyanine signal, and then fixed and permeabilized the cells to stain for phospho-H2AX and re-imaged the same cells. To obtain a more optimal signal,

fixed permeabilized cells were stained with an anti-Cy3 antibody to detect RhPPO-Cy3. In co-staining experiments with phospho-H2AX, the nuclear RhPPO-Cy3 foci exhibited partial overlap with phospho-H2AX foci (20 ± 4%) (Figure 3B), suggesting that the DNA lesions formed by RhPPO-Cy3 binding occur at or near sites of DNA mismatches.

Phospho-H2AX, as a component of chromatin, spans megabases of DNA surrounding a DNA break.[32] To explore further the potential colocalization of RhPPO-Cy3 with DNA damage foci, we compared RhPPO-Cy3 nuclear localization to that of Rad51, a strand exchange enzyme that binds single-stranded DNA (ssDNA) formed from resection of DNA DSBs.[33] RhPPO-Cy3 foci showed strong overlap with Rad51 foci (24 ± 6%)(Figure 3C). Neutral comet assays confirmed that RhPPO-Cy3 treatment induced DNA DSBs (Supplemental Information, Figure S11). After 24 hours treatment with 5 μM RhPPO-Cy3, HCT-116 O and HCT-116 N cells analyzed by TBE electrophoresis exhibited Comet tails indicating the presence of DNA damage; 29.1 ± 6.7 % of the MMR-deficient HCT-116 O cells displayed Comet tails, compared to 18.9 ± 3.9 % of HCT-116 N cells. These findings further support the idea that RhPPO-Cy3 binding to cellular DNA mismatches generates DNA damage at or near the mismatch site.

The DNA lesions induced by RhPPO-Cy3 could be a direct consequence of the complex binding to a mismatch (*e.g.* by causing extrusion of the mismatched base pair and activation of a DNA-binding protein, generating damage) or could result indirectly as cells attempt to unwind the DNA helix for replication or transcription. To test these

possibilities, HCT-116 O and HCT-116 N cells were treated with the CDK4/6 inhibitor palbociclib for 24 hours to induce G1/S phase arrest, and then cell killing by RhPPO-Cy3 was compared in cells maintained in cell cycle block versus cells where the inhibitor was washed out to allow cell cycle progression. RhPPO-Cy3 was cytotoxic to cells treated with palbociclib, and the cell killing was further increased when cells re-entered the cell cycle and palbociclib was washed out (Figure 4A). The cytotoxicity observed was due to RhPPO-Cy3 treatment, as little to no cell killing occurred in the absence of the compound. Cytotoxicity mediated by cisplatin was increased in cycling cells, consistent with its known mechanism of action. These studies suggest that RhPPO-Cy3 induces DNA damage directly upon binding to cellular DNA mismatches.

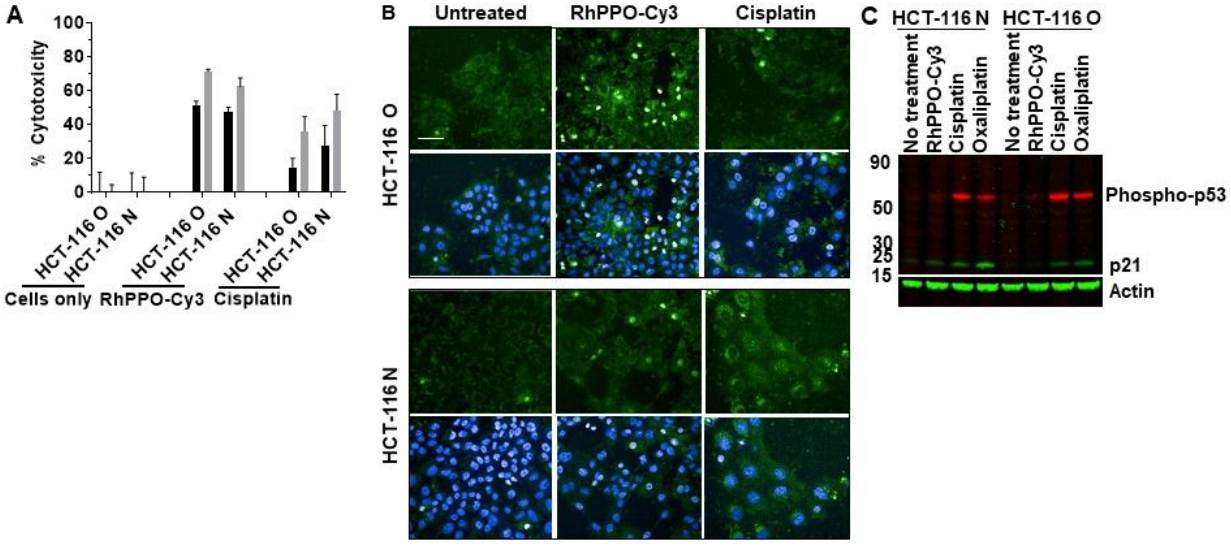

Figure 4. RhPPO-Cy3 does not activate p53/ p21 to initiate apoptosis. HCT-116 O and HCT-116 N cells were treated with 5 μM RhPPO-Cy3 and analyzed for mechanism of cell death. (A) RhPPO-Cy3 induces cell death in cells arrested in G1/ S phase as well as

in cycling cells. Cells were blocked in G1/S using 1 mM palbociclib, then RhPPO-Cy3 or cisplatin was added to cells held in arrest (black bars) or released back into the cell cycle (gray bars). Cell viability was assessed by CellTiter-Glo. Results from duplicate samples from a representative experiment are shown. (B) Cells that were untreated, or treated with 5 μM RhPPO-Cy3 or 36 μM cisplatin for 24 hours, were stained for Nuclear Green DCS dye as a marker for necrosis. Live cells were visualized with Hoechst dye. Scale bar, 20 μm. (C) Protein lysates were prepared from HCT-116 O and HCT-116 N cells that were untreated, or treated with 5 mM RhPPO-Cy3, 36 μM cisplatin, or 25 μM oxaliplatin for 24 hours. 40 μg of protein was analyzed for phospho-p53 and total p21 proteins. Blots were also probed for actin to confirm similar amounts of protein in each sample.

RhPPO-Cy3 does not activate the p53-dependent apoptotic response. In time course studies, we observed that the RhPPO-Cy3-induced nuclear damage foci persisted until cell death occurred. Imaging analysis of the mechanism of cell death showed that RhPPO-Cy3 treatment led to necrosis, unlike cisplatin which causes very little necrotic cell death (Figure 4B). Consistent with these findings, RhPPO-Cy3 treatment did not lead to activation or accumulation of the p53 protein (Figure 4C). RhPPO-Cy3 also did not induce p21, a downstream target of p53 that mediates cell cycle arrest. In contrast, HCT-116 O and HCT-116 N cells underwent apoptosis in

response to DNA damage induced by cisplatin treatment (Figure 4C), suggesting that the lesions caused by RhPPO-Cy3 binding do not trigger a cell cycle checkpoint or the apoptotic pathway. These results support the hypothesis that the DNA lesions induced by RhPPO-Cy3 binding to DNA mismatches are not able to be repaired in the presence of the compound and also prevent cross-talk between DNA checkpoint proteins and p53, the key mediator of the apoptotic pathway.

DISCUSSION

DNA mismatches present in MMR-deficient cancer cells present an opportunity for selective therapeutic targeting. The rhodium metalloinsertor RhPPO is characterized by high cellular potency across MMR-deficient cell lines,[22, 24] and we have proposed that its buckled orientation in the DNA minor groove leads to a pronounced extrusion of the mismatched base pair from the DNA helix that activates DNA-binding proteins to generate DNA lesions.[22, 23] Crystallography efforts are ongoing to address the molecular structure of RhPPO bound to the DNA mismatch. As an alternative approach, we generated a fluorescent conjugate of RhPPO to enable direct visualization of the compound binding and activity within cells.

Our first-generation fluorescent probe, RhCy3, demonstrated fluorescence intensity that correlated with the presence of DNA mismatches and with RhPPO cytotoxicity[24]. In the current study, we directly labeled RhPPO with a fluorescent

conjugate to generate RhPPO-Cy3. This probe exhibited similar binding affinity, cell activity and selectivity as RhPPO, indicating that the fluorescent conjugate has appropriate characteristics to enable studies of the cellular mechanism of action. RhPPO-Cy3 enabled the first direct visualization of rhodium metalloinsertor localization to discrete foci within the cell nucleus and overlapped with DNA damage foci containing phospho-H2AX and Rad51. These data support the idea that RhPPO/RhPPO-Cy3 binds DNA mismatches in nuclear DNA and generates DNA damage at or near the DNA mismatch site upon binding. RhPPO-Cy3 selective cytotoxicity is observed in cell lines with mutation or inactivation of MLH1, MSH2 or other MMR genes, consistent with the rhodium metalloinsertor targeting the state of MMR deficiency.

RhPPO-Cy3 activates the DNA damage checkpoint and recruits Rad51, suggesting that the lesions include DNA DSBs that undergo initial processing to form regions of single-stranded DNA. Although RhPPO-Cy3 binding is noncovalent, the foci persist over time, suggesting that the mismatch site remains unrepaired as long as the compound is present. The DNA lesion may involve the mismatched base pairs and could require MMR for repair. However, RhPPO-Cy3 foci persist both in HCT-116 O and HCT-116 N cells, suggesting that MMR is not a major mechanism for repair of the lesions. Instead, the lesions may activate the nucleotide excision repair (NER) pathway, which recognizes bulky lesions that distort the DNA helix, independent of sequence or

DNA structure.[34] Repair by NER requires verification of the DNA damage.[35] The lesions caused by RhPPO-Cy3 also might be in a chromosomal context that is not accessible to NER or other DNA repair enzymes. MMR-deficient cancer cells often have mutations in genes involved in DNA repair.[36] Alternatively, the cell cycle block resulting from RhPPO-Cy3 binding may inhibit recruitment of appropriate repair factors to the DNA lesions. Interestingly, RhPPO-Cy3-induced DNA damage does not lead to upregulation of p53 or p21, which mediate checkpoint-dependent cell cycle arrest and apoptosis. We propose that RhPPO-Cy3 binding leads to necrosis as a default cell death pathway after the irreparable DNA lesions fail to induce cell death by apoptosis. A model for the RhPPO-Cy3 mechanism of action is shown in Figure 5.

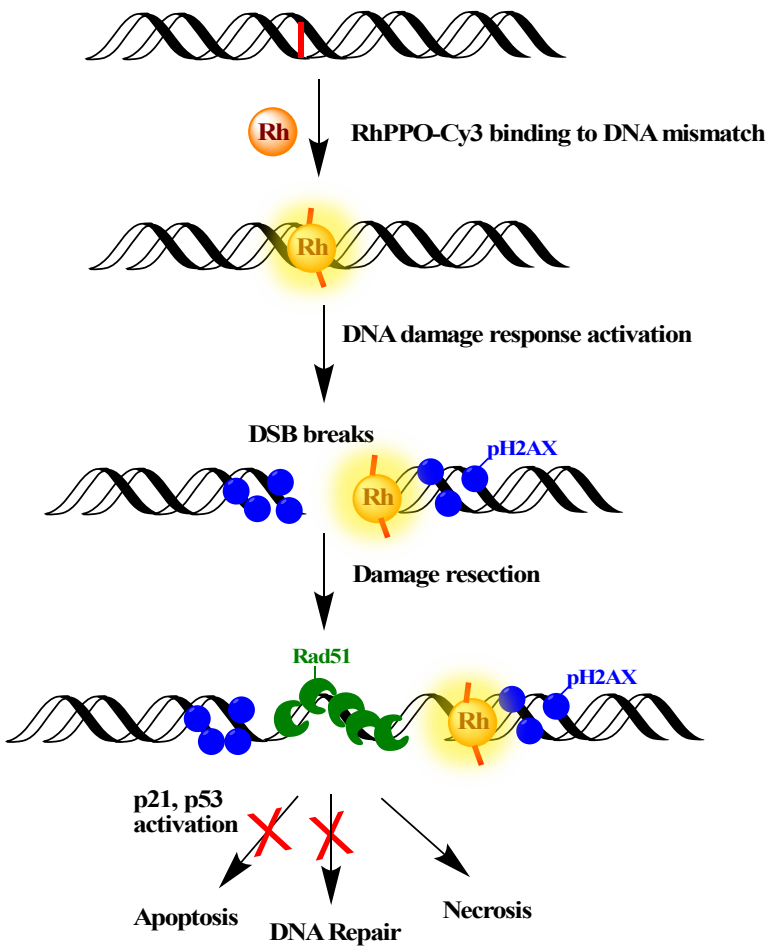

Figure 5. Model for RhPPO-Cy3 mechanism of action of cytotoxicity. Mismatch binding generates DNA damage that activates pH2AX and Rad51, indicating DSBs form and undergo initial resection. Further repair of the lesion does not occur, potentially due to inaccessibility to the lesion or a physical block to cell cycle progression. Cells are unable to signal the damage to p53 to trigger apoptosis. Instead, the primary mode of cell death is necrosis. See text for additional details.

CONCLUSION

Targeting of DNA mismatches with rhodium metalloinsertors such as RhPPO provides a therapeutic approach that is distinct from current strategies such as platinum-based chemotherapy or immune checkpoint blockade with anti-PD-1 antibodies. RhPPO-Cy3, as a fluorescent analog, provides a means to probe the mechanism of action of these rhodium metalloinsertors in detail. The rhodium complexes yield DNA lesions that promote the recruitment of repair proteins but do not trigger the canonical damage-induced apoptosis pathway nor to the activation of p53. This response to DNA damage raises the possibility that cells may be less likely to develop resistance to metalloinsertors than occurs with standard chemotherapy. RhPPO and RhPPO-Cy3 thus enable the molecular detection of cellular mismatches and antitumor activity with high cell selectivity. This strategy therefore provides a differentiated therapeutic option for the treatment of MMR-deficient cancers.

ASSOCIATED CONTENT

Supporting Information.

The following file is available free of charge on the ACS Publications website: The file contains all the characterization spectra (*i.e.* NMR, MS, UV-vis, HPLC) and additional data on RhPPO-Cy3 cellular cytotoxicity.

AUTHOR INFORMATION

Corresponding Authors

*Julie M. Bailis, Ph.D., Department of Oncology Research, Amgen Research, Amgen, Inc., South San Francisco, CA 94080. Email: jbailis@amgen.com; Telephone: +1 (650) 244 2361.

*Jacqueline K. Barton, Ph.D., Division of Chemistry and Chemical Engineering, California Institute of Technology, Pasadena, CA 91125. Email: jkbarton@caltech.edu; Telephone: +1 (626) 395-6075; Fax: +1 (626) 577-4976.

Funding

This work was supported by funding from Amgen and from the Moore Foundation.

Notes

The authors declare no competing financial interests.

ACKNOWLEDGEMENTS

We are grateful to the Moore Foundation and the Beckman Laser Resources Center for their support. We thank Christopher Hale (Amgen) for technical assistance with image analysis.

REFERENCES

1. Modrich, P.; Lahue, R. (**1996**) Mismatch repair in replication fidelity, genetic recombination, and cancer biology. *Annu. Rev. Biochem. 65*, 101-133.

2. a) Kunkel, T. A.; Erie, D. A. (**2005**) DNA mismatch repair. *Annu. Rev. Biochem. 74*, 681-710. b) Li, G. M. (**2008)** Mechanisms and functions of DNA mismatch repair. *Cell Res. 18*, 85-98.

3. Richman, S. (**2015**) Deficient mismatch repair: Read all about it (Review). *Int. J. Oncol. 47*, 1189-1202.

4. Herman, J. G.; Umar, A.; Polyak, K.; Graff, J. R.; Ahuja, N.; Issa, J.-P. J.; Markowitz, S.; Willson, J. K. V.; Hamilton, S. R.; Kinzler, K. W.; Kane, M. F.; Kolodner, R. D.; Vogelstein, B.; Kunkel, T. A.; Baylin, S. B. (**1998)** Incidence and functional consequences of hMLH1 promoter hypermethylation in colorectal carcinoma. *Proc. Natl. Acad. Sci. U. S. A. 95*, 6870-6875.

5. Hatch, S. B.; Lightfoot Jr., H. M.; Garwackie, C. P.; Moore, D. T.; Calvo, B. F.; Woosley, J. T.; Sciarrotta, J.; Funkhouser, W. K.; Farber, R. A. (**2005**) Microsatellite instability testing in colorectal carcinoma: choice of markers affects sensitivity of detection of mismatch repair-deficient tumors. *Clin. Can. Res. 1*, 2180-2187.

6. Guinney, J.; Dienstmann, R.; Wang, X.; De Reyniès, A.; Schlicker, A.; Soneson, C.; Marisa, L.; Roepman, P.; Nyamundanda, G.; Angelino, P.; Bot, B. M.; Morris, J. S.; Simon, I. M.; Gerster, S.; Fessler, E.; De Sousa, E.; Melo, F.; Missiaglia, E.; Ramay, H.; Barras, D.; Homicsko, K.; Maru, D.; Manyam, G. C.; Broom, B.; Boige, V.; Perez-Villamil, B.; Laderas, T.; Salazar, R.; Gray, J. W.; Hanahan, D.; Tabernero, J.; Bernards, R.; Friend, S. H.; Laurent-Puig, P.; Medema, J. P.;

Sadanandam, A.; Wessels, L.; Delorenzi, M.; Kopetz, S.; Vermeulen, L.; Tejpar, S. (**2015**) The consensus molecular subtypes of colorectal cancer. *Nat. Med. 21*, 1350-1356.

7. Bonneville, R.; Krook, M. A.; Kautto, E. A.; Miya, J.; Wing, M. R.; Chen, H. Z.; Reeser, J. W.; Yu, L.; Roychowdhury, S. (**2017**) Landscape of Microsatellite Instability Across 39 Cancer Types. *JCO Precis. Oncol.* doi: 10.1200/PO.17.00073.
8. Germano, G.; Amirouchene-Angelozzi, N.; Rospo, G.; Bardelli, A. (**2018**) The Clinical Impact of the Genomic Landscape of Mismatch Repair–Deficient Cancers. *Cancer Discov*. *12*, 1518-1528.
9. Fountzilas, E.; Kotoula, V.; Pentheroudakis, G. Manousou, K.; Polychronidou, G.; Vrettou, E.; Poulios, C.; Papadopoulou, E.; Raptou, G.; Pectasides, E.; Karayannopoulou, E.; Chrisafi, S.; Papakostas, P.; Makatsoris, T.; Varthalitis, I.; Psyrri, A.; Samantas, E.; Bobos, M.; Christodoulou, C.; Papadimitriou, C.; Nasioulas, G.; Pectasides, D.; Fountzilas, G. (**2019**) Prognostic implications of mismatch repair de ciency in patients with nonmetastatic colorectal and endometrial cancer. *ESMO Open 4*, e000474. doi:10.1136/esmoopen-2018-000474.
10. Sargent, D. J.; Marsoni, S.; Monges, G.; Thibodeau, S. N.; Labianca, R.; Hamilton, S. R.; French, A.J.; Kabat, B.; Foster, N. R.; Torri, V.; Ribic, C.; Grothey, A.; Moore, M.; Zaniboni, A.; Seitz, J. F.; Sinicrope, F.; Gallinger, S. (**2010**) Defective mismatch

repair as a predictive marker for lack of efficacy of fluorouracil-based adjuvant therapy in colon cancer. *J. Clin. Oncol. 28*, 3219-3226.

11. Guastadisegni, C.; Colafranceschi, M.; Ottini, L.; Dogliotti, E. (**2010**) Microsatellite instability as a marker of prognosis and response to therapy: a meta-analysis of colorectal cancer survival data. *Eur. J. Cancer*, *46*, 2788-2798.
12. Le, D. T.; Durham, J. N.; Wang, H.; Bartlett, B. R.; Kemberling, H.; Eyring, A. D.; Skora, A. D.; Luber, B. S.; Azad, N. S.; Laheru, D.; Biedrzycki, B.; Donehower, R. C; Zaheer, A.; Fisher, G. A.; Crocenzi, T. S.; Lee, J. J.; Duffy, S. M.; Goldberg, R. M; Chapelle, A. de la; Koshiji, M; Bhaijee, F.; Huebner, T.; Hruban, R. H.; Wood, L. D.; Cuka, N.; Pardoll, D. M.; Papadopoulos, N.; Kinzler, K. W.; Zhou, S.; Cornish, T. C.; Taube, J. M.; Anders, R. A.; Eshleman, J. R.; Vogelstein, B.; Diaz, L. A. Jr. (**2015**) PD-1 Blockade in Tumors with Mismatch-Repair Deficiency. *N. Engl. J. Med. 372*, 2509-2520.
13. Le, D. T.; Durham, J. N.; Smith, K. N.; Wang, h.; Bartlett, B. R.; Aulakh, L. K.; Lu, S. Kemberling, K.; Wilt, C.; Luber, B. S.; Wong, F.; Azad, N. S.; Rucki, A. A.; Laheru, D.; Donehower, R.; Zaheer, A.; Fisher, G. A.; Crocenzi, T. S.; Lee, J. J.; Greten, T. F.; Duffy, A. G.; Ciombor, K. K.; Eyring, A. D.; Lam, B. H.; Joe, A.; Kang, S. P.; Holdhoff, M.; Danilova, L.; Cope, L.; Meyer, C.; Zhou, S.; Goldberg, R. M.; Armstrong, D. K.; Bever, K. M.; Fader, A. N.; Taube, J.; Housseau, F.; Spetzler, D.; Xiao, N.; Pardoll, D. M.; Papadopoulos, N.; Kinzler, K. W. Eshleman, J. R.; Vogelstein, B.; Anders, R. A.;

Diaz Jr., L. A. (**2017**) Mismatch-repair deficiency predicts response of solid tumors to PD-1 blockade. *Science 357*, 409-413.

14. Nguyen, K.; Mason, R.; Ladwa, R.; Warburton, L.; Millward, M.; Haydon, A. M.; Carlino, M. S.; Smith, J. L.; Atkinson, V. (**2018**) Relapse after cessation of PD-1 based therapy for complete responders in metastatic melanoma. *J. Clin. Oncol. 36*, 9536-9536.

15. Larkin, J.; Chiarion-Sileni, V.; Gonzalez, R.; Grob, J. J.; Cowey, C. L.; Lao, C. D.; Schadendorf, D.; Dummer, R.; Smylie, M.; Rutkowski, P.; Ferrucci, P. F.; Hill, A.; Wagstaff, J.; Carlino, M. S.; Haanen, J. B.; Maio, M.; Marquez-Rodas, I.; McArthur, G. A.; Ascierto, P. A.; Long, G. V.; Callahan, M. K.; Postow, M. A.; Grossmann, K.; Sznol, M.; Dreno, B.; Bastholt, L.; Yang, A.; Rollin, L. M.; Horak, C.; Hodi, F. S.; Wolchok, J. D. (**2015**) Combined Nivolumab and Ipilimumab or Monotherapy in Untreated Melanoma. *N. Engl. J. Med. 372*, 2006-2017.

16. Wolchok, J. D.; Chiarion-Sileni, V.; Gonzalez, R.; Rutkowski, P.; Grob, J.-J.; Cowey, C. L.; Lao, C. D.; Wagstaff, J.; Schadendorf, D.; Ferrucci, P. F.; Smylie, M.; Dummer, R.; Hill, A.; Hogg, D.; Haanen, J.; Carlino, M. S.; Bechter, O.; Maio, M.; Marquez-Rodas, I.; Guidoboni, M.; McArthur, G.; Lebbé, C.; Ascierto, P. A.; Long, G. V.; Cebon, J.; Sosman, J.; Postow, M. A.; Callahan, M. K.; Walker, D.; Rollin, L.; Bhore, R.; Hodi, F. S.; Larkin, J. (**2017**) Overall Survival with Combined Nivolumab and Ipilimumab in Advanced Melanoma. *N. Engl. J. Med. 377*, 1345-1356.

17. Hart, J. R.; Glebov, O.; Ernst, R. J.; Kirsch., I. R.; Barton, J. K. (2006) DNA mismatch-specific targeting and hypersensitivity of mismatch-repair-deficient cells to bulky rhodium(III) intercalators. *Proc. Natl. Acad. Sci. U. S. A. 103*, 15359-15363.

18. Zeglis, B.M.; Pierre, V. C.; Barton, J. K. (**2007**) Metallointercalators and Metalloinsertors. *Chem. Comm. 44,* 4565-4579.

19. Pierre, V. C.; Kaiser, J. T.; Barton, J. K. (**2007**) Insights into finding a mismatch through the structure of a mispaired DNA bound by a rhodium intercalator. *Proc. Natl. Acad. Sci. U. S. A. 104*, 429-434.

20. Ernst, R. J.; Komor, A. C.; Barton, J. K. (**2011**) Selective cytotoxicity of rhodium metalloinsertors in mismatch repair-deficient cells. *Biochemistry 50,* 10919-10928.

21. Komor, A. C.; Barton, J. K. (**2014**) An Unusual Ligand Coordination Gives Rise to a New Family of Rhodium Metalloinsertors with Improved Selectivity and Potency. *J. Am. Chem. Soc. 136*, 14160-14172.

22. Boyle, K. M.; Barton, J. K. (**2018**) A Family of Rhodium Complexes with Selective Toxicity toward Mismatch Repair-Deficient Cancers. *J. Am. Chem. Soc. 140*, 5612-5624.

23. Bailis, J. M.; Weidmann, A. G.; Mariano, N. F.; Barton, J. K. (**2017**) Rhodium metalloinsertor binding generates a lesion with selective cytotoxicity for mismatch repair-deficient cells. *Proc. Natl. Acad. Sci. U. S. A. 114*, 6948-6953.

24. Boyle, K. M.; Nano, A.; Day, C.; Barton, J. K. (**2019**) Cellular Target of a Rhodium Metalloinsertor is the DNA Base Pair Mismatch. *Chem. Eur. J. 25*, 3014-3019.

25. Nano, A.; Boynton, A.; Barton, J.K. (**2017**) A Rhodium-Cyanine Fluorescent Probe: Detection and Signaling of Mismatches in DNA. *J. Am. Chem. Soc. 139*, 17301-17304.

26. Dasari, S.; Tchounwou, P. B. (**2014**) Cisplatin in cancer therapy: molecular mechanisms of action. *Eur. J. Pharmacol. 740*, 364-378.

27. Tacar, O.; Sriamornsak, P.; Dass, C. R. (**2013**) Doxorubicin: an update on anticancer molecular action, toxicity and novel drug delivery systems. *J. Pharm. Pharmacol. 56*,157-70.

28. Ernst, R. J.; Song, H.; Barton, J. K. (**2009**) DNA Mismatch Binding and Antiproliferative Activity of Rhodium Metalloinsertors. *J. Am. Chem. Soc. 131*, 2359-2366.

29. a) Hulme, E. C.; Trevethick, M. A. (**2010**) Ligand binding assays at equilibrium: validation and interpretation. *Br. J. Pharmacol. 161*, 1219-1237. b) Pollard, T. D. (**2010**) A guide to simple and informative binding assays. *Mol. Biol. Cell. 21*, 4061-4067.

30. Koi, M.; Umar, A.; Chauhan, D. P.; Cherian, S. P.; Carethers, J. M.; Kunkel, T. A.; Boland, C. R. (**1994**) Human chromosome 3 corrects mismatch repair deficiency and microsatellite instability and reduces N-methyl-N′-nitro-N-nitrosoguanidine

tolerance in colon tumor cells with homozygous hMLH1. *Cancer Res. 54*, 4308-4312.

31. Bailis, J. M.; Gordon, M. L.; Gurgel, J. L.; Komor, A. C.; Barton, J. K.; Kirsch, I. R. (**2013**) An inducible, isogenic cancer cell line system for targeting the state of mismatch repair deficiency. *PLoS One 8*, e78726. doi: 10.1371/journal.pone.0078726.
32. Rogakou, E. P.; Boon, C.; Redon, C.; Bonner, W. M. (**1999**) Megabase Chromatin Domains Involved in DNA Double-Strand Breaks in Vivo. *J. Cell. Biol.* 146, 905-916.
33. Paull, T. T.; Rogakou, E. P.; Yamazaki, V.; Kirchgessner, C. U.; Gellert, M.; Bonner, W. M. (**2000**) A critical role for histone H2AX in recruitment of repair factors to nuclear foci after DNA damage. *Curr. Biol. 10*, 886-895.
34. Mu, H.; Geacintov, N. E.; Broyde, S.; Yeo, J.-E.; Schärer, O. D. (**2018**) Molecular basis for damage recognition and verification by XPC-RAD23B and TFIIH in nucleotide excision repair. *DNA Repair 17*, 33-42.
35. Marteijn, J. A.; Lans, H.; Vermeulen, W.; Hoeijmakers, J. H. (**2014**) Understanding nucleotide excision repair and its roles in cancer and ageing. *Nat. Rev. Mol. Cell. Biol. 15*, 465-481.
36. Miquel, C.; Jacob, S.; Grandjouan, S.; Aimé, A.; Viguier, J.; Sabourin, J.-C.; Sarasin, A.; Duval, A.; Praz, F. (**2007**) Frequent alteration of DNA damage

signalling and repair pathways in human colorectal cancers with microsatellite instability. *Oncogene 26*, 5919-5926.

For Table of Contents use only